Carbon 197 (2022) 435–443

Contents lists available at ScienceDirect

Carbon

journal homepage: www.elsevier.com/locate/carbon

Graphitization vs tribo-oxidation governing friction behaviors of doped graphene nanocrystalline carbon films

Cheng Chen, Peidong Xue, Dongfeng Diao *

Institute of Nanosurface Science and Engineering (INSE), Guangdong Provincial Key Laboratory of Micro/Nano Optomechatronics Engineering, Shenzhen University, Shenzhen, 518060, China

ARTICLE INFO

Keywords:
Carbon film
Friction
Graphitization
Tribo-oxidation

ABSTRACT

Graphitization and tribo-oxidation are two common phenomena found at the friction interfaces of carbon-based films in atmospheric environment. However, the specific contributions of them to the low friction behavior are not well clarified. Here, we show two kinds of low friction behaviors of graphene nanocrystalline carbon (GNC) films doped with different elements (Ti, Al, Si). The promotion effects of graphene nanocrystallites on the graphitization and different doping elements on the tribo-oxidation were detailed analyzed for uncovering the low friction mechanisms. The results suggest that the relationship between graphitization and tribo-oxidation could be competitive or coexisting. For competitive type, the friction coefficient of Ti-doped GNC film first decreased to a low-friction stage due to graphitization, and then gradually increased into a steady-friction stage by tribo-oxidation. For coexisting type, the graphitization and tribo-oxidation co-induced the steady-low-friction behaviors of Al-doped and Si-doped GNC films. This work provides new insights into the friction mechanism, and the guidance for the design of doped GNC films with desired friction behaviors.

1. Introduction

Amorphous carbon (a-C) film is an important class of tribological materials for its excellent properties such as low friction coefficient, high wear resistance and hardness [1–3]. Over the past decades, it has been extensively studied and used in widespread applications, such as magnetic disks, razor blades, automobile engines, cutting tools, space-based technologies, and micro-electro-mechanical systems [2–4]. Nowadays, it still attracts enormous interests from scientific and industrial communities to modify the structure of amorphous carbon film in nanoscale for improving or extending the properties of the film [5–10].

The low friction of a-C film, especially the hydrogen free a-C film, has been mainly attributed to the friction-induced graphitization of contact surface and the consequent formation of a graphitelike nanocrystallite tribofilm on the sliding surface of the counterpart [11–13]. The tribofilm lowers the interaction force between the sliding surfaces from strong covalent bonds to mainly weak van der Waals forces. However, the formation of graphitelike nanocrystallite tribofilm is strongly dependent on many factors, such as normal load, sliding velocity, counterpart material, atmosphere, as well as the structural, chemical, and mechanical properties of the a-C film [14–18]. Therefore, in some cases, a-C film cannot reach a low friction state, or need to go through a long period of high friction run-in stage to enter the low friction state [6,18]. In order to ensure or optimize the low friction performance of a-C film, many strategies have been proposed to promote the graphitization of sliding surfaces. For instance, doping the a-C film with additional elements [19,20], embedding the a-C film with sp2 nanocrystallites [5,6], applying an external electric current to the friction system [21,22].

In fact, it should be noted that the sliding friction process of carbon film in atmospheric environment is inevitably accompanied by tribo-oxidation to some extent. The effect of tribo-oxidation on the friction behavior is worthy of in-depth discussion, although it is not regarded as a determining factor for the low friction. On one hand, the tribo-oxidation by water or oxygen can help to passivate the carbon surface dangling bonds [23]. On the other hand, it might increase the wear and destroy the graphene nanostructure [24]. And those effects become more complicated for the carbon films doped with additional elements. Some doped elements are more likely to oxidize under sliding friction and form different oxides, which might accumulate at the sliding interface and participate in the formation of tribofilm [25,26]. In this case, it seems to be insufficient and hasty to explain the low friction behavior simply by graphitization. In other words, whether

* Corresponding author.
E-mail address: dfdiao@szu.edu.cn (D. Diao).

https://doi.org/10.1016/j.carbon.2022.07.001
Received 4 May 2022; Received in revised form 30 June 2022; Accepted 1 July 2022
Available online 2 July 2022

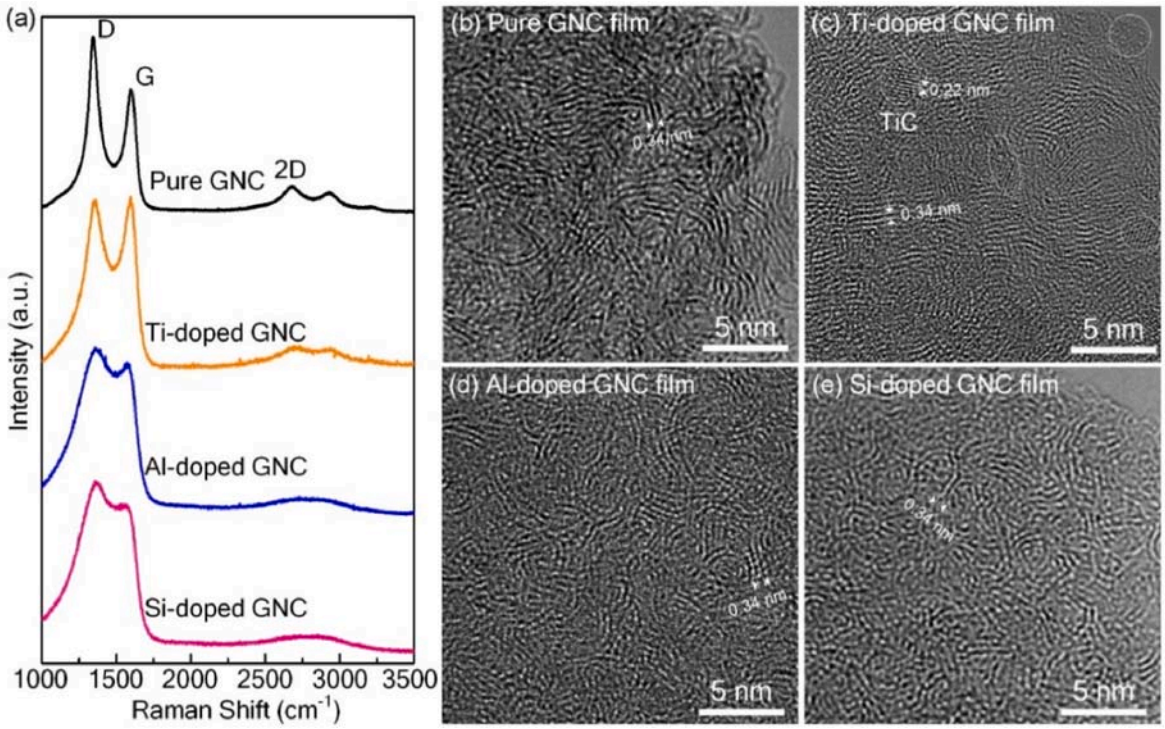

Fig. 1. (a) Raman spectra of pure GNC film and doped GNC films (doping target current: 0.7 A). Plan TEM images of (b) pure GNC film, (c) Ti-doped GNC film, (d) Al-doped GNC film, and (e) Si-doped GNC film. (A colour version of this figure can be viewed online.)

graphitization can be regarded as the only design basis for the optimization of low friction performance of doped carbon films or not? Hence, it is necessary to clarify the specific effects of graphitization and tribo-oxidation on the friction behavior of doped carbon films.

In this research, we study the friction behaviors of graphene nanocrystalline carbon (GNC) films doped with different elements (Ti, Al, Si), with particular emphasis on the effects of graphitization and tribo-oxidation on the friction behavior and especially on the formation of tribofilm. Due to the abundant graphene nanocrystallites embedded in the GNC film, the friction induced graphitization could occur easier and faster compared with the a-C film [6], which is helpful to clarify the specific effects of graphitization and tribo-oxidation. Our results show that the friction behaviors of the doped GNC films were strongly influenced by graphitization and tribo-oxidation, and were mainly dependent on the tribofilm formation during sliding. Tribo-oxidation is not always antithetical to low friction, and can sometimes coexist with graphitization to promote low friction together.

2. Experimental section

2.1. Film fabrication

The pure and doped GNC films were deposited on silicon substrate (p-type <100>) by using a hybrid sputtering system with an electron cyclotron resonance (ECR) plasma sputtering for carbon deposition and a magnetron sputtering for different element doping. The detailed descriptions of the sputtering system were reported in our previous works [27,28]. The background pressure of the vacuum chamber was 8×10^{-5} Pa, and the argon working pressure was kept at 1×10^{-1} Pa. During the film deposition, low-energy electron irradiation on the film was realized by applying a positive bias voltage of +80 V to the substrate, inducing the formation of graphene nanocrystallites. Different elements doping of Ti, Al, and Si was realized by changing magnetron sputtering targets. Magnetron target currents were set as 0.1 A, 0.3 A, 0.5 A and 0.7 A to obtain different doping concentrations. The film thicknesses were ~150 nm controlled by deposition time. The deposition rates were about 5–6 nm/min for different doping parameters, which are estimated with a stylus profilometer (Bruker, Dektak-XT) and the cross-sectional view TEM images of the films [27].

2.2. Characterization

The nanostructures of the pure and doped GNC films were analyzed with a Raman spectroscopy (HORIBA, HR-Resolution; wavelength of 532 nm) and a Cs-corrected transmission electron microscope (TEM, Thermo Fisher Scientific, Titan3 Themis G2). The TEM was operated at 80 kV to avoid possible damages or recrystallization caused by electron irradiation. The plan view TEM specimens were prepared by scratching the film surface with a diamond pencil to form carbon flakes, which were then transferred onto copper micro grids. The cross-sectional view TEM specimens of the tribofilms were fabricated by using a focused ion beam (FIB, Thermo Fisher Scientific, Scios). The chemical compositions of films were analyzed using an AXIS ultra DLD multifunctional XPS with a monochromatic Al Ka Xray source. For the Ti-doped, Al-doped, and Si-doped GNC films fabricated with doping target current of 0.7 A, the doping concentrations of Ti, Al and Si were ~4.8 at.%, ~21.7 at.% and ~11.6 at.%, respectively (See Fig. S1 in the Supplementary data).

The friction tests of films sliding against a Si_3N_4 ball (radius of 3.17 mm) were performed with a Pin-on-Disk tribometer. The normal load was 2 N. The sliding velocity was 26.4 mm/s, corresponding to a constant disk rotational speed of 180 rpm with a frictional radius of 1.4 mm. The tests were operated in a clean room with a temperature of 24 °C and a relative humidity of 45–50%.

3. Results and discussion

3.1. Film nanostructure

Fig. 1 shows Raman spectra and plan view TEM images of the pure GNC and doped GNC films. For the pure GNC film, the Raman spectrum exhibits three sharp bands of D band, G band and 2D band respectively around 1340, 1590 and 2700 cm^1, confirming the existence of graphene

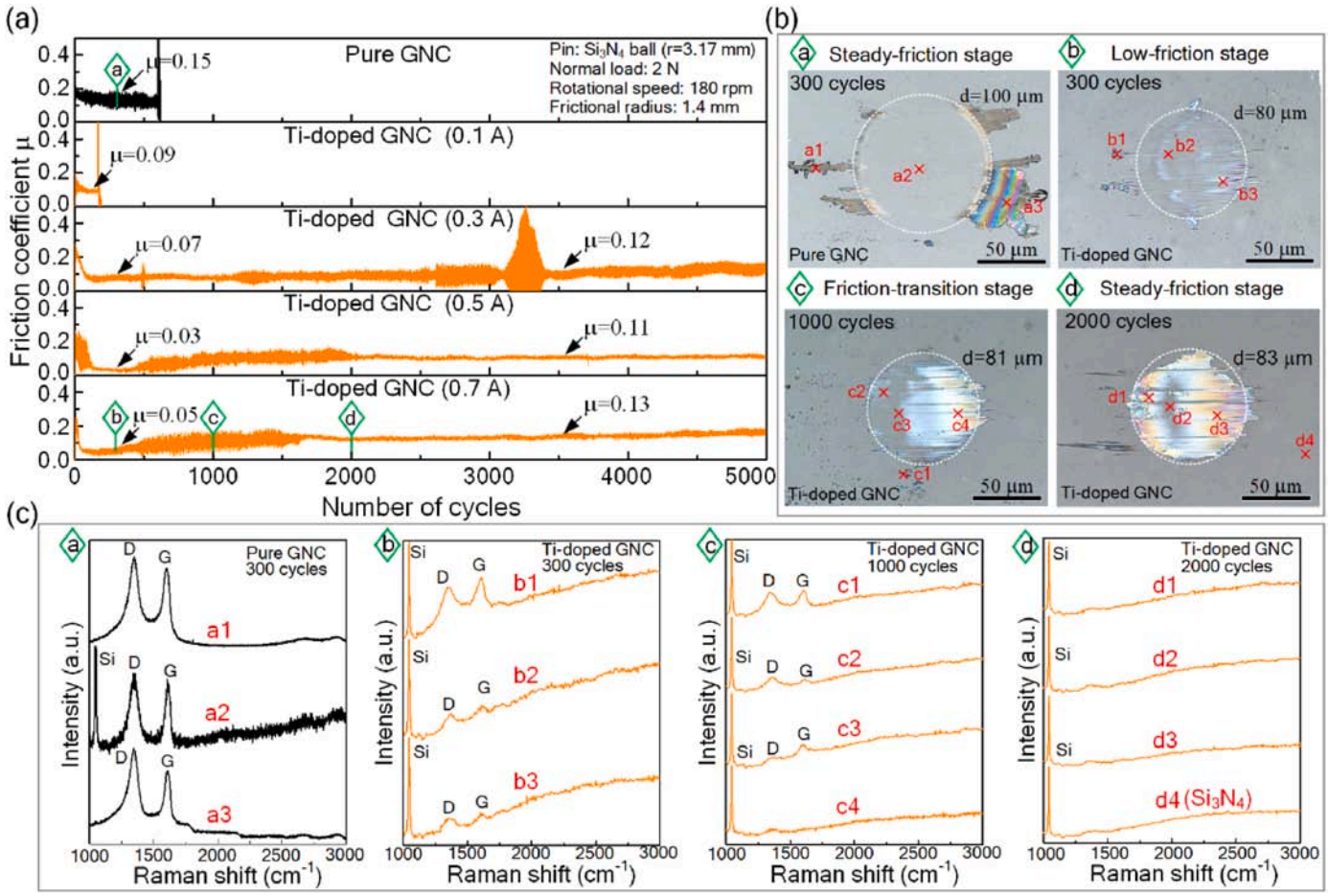

Fig. 2. (a) Typical friction curves of pure GNC film and Ti-doped GNC films with different Ti target currents. (b) Optical images of worn scars on the Si_3N_4 ball surfaces after different sliding cycles indicated in Fig. 2(a). (c) Raman spectra of the worn scars on the Si_3N_4 ball surfaces indicated in Fig. 2(b). (A colour version of this figure can be viewed online.)

nanocrystallites [29,30]. After element doping, the shapes of D and G bands became coupling and the relative intensities of 2D bands decreased, which indicates the decrease of graphene nanocrystallite size. From the TEM images, all the films contain randomly oriented graphene nanocrystallites embedded in the amorphous carbon matrix. The graphene nanocrystallites in the doped GNC films (Fig. 1c–e) appear to be smaller than that of the pure GNC film (Fig. 1b), which is in accordance with the analysis results of Raman spectra. And it should be noticed that Ti-doping induced the formation of TiC nanocrystallites, as marked with white circles in Fig. 1c. For Al-doping and Si-doping GNC films, no nanocrystalline carbides can be found in the TEM images (Fig. 1 d-e).

3.2. Friction behaviors of Ti-doped GNC films

Fig. 2a shows the typical friction curves of pure GNC film and Ti-doped GNC films fabricated with different Ti target currents. The friction coefficient of the pure GNC film was ~0.15 after the run-in stage, then suddenly increased after ~600 sliding cycles, indicating the failure of the film. For the Ti-doped GNC film with Ti target current of 0.1 A, the friction coefficient was 0.09 and wear life was ~160 cycles. When the Ti target current was 0.3 A and over, the wear life increased to more than 5000 cycles. And the friction curves showed four distinct stages: run-in stage, low-friction stage, friction-transition stage, and steady-friction stage. For example, the fiction coefficient of the Ti-GNC film with Ti target current of 0.7 A first decreased to a low value of 0.05 after about 50 sliding cycles, then gradually increased to another steady value of 0.13 after about 1700 cycles. And it can be found that the periods of the low friction stage and friction-transition stage decreased with the increasing of Ti target current.

In order to understand the friction behaviors, the structures of worn scars on the Si_3N_4 ball surfaces after 300, 1000 and 2000 cycles were observed and analyzed with an optical microscope and Raman spectroscopy. The results are shown in Fig. 2b–c. Tribofilms can be found on each ball surface (see Fig. 2b). For the tribofilm of GNC film, the wear debris mainly accumulated at the outsides of the central contact area. Whereas, the tribofilms of Ti-doped GNC films mostly formed at the central contact areas. And it can be observed that the silvery area increased with the sliding cycles. After 2000 cycles sliding, the tribofilm was mainly composed of silvery material. To investigate the chemical compositions, elemental mapping analyses were carried out with energy dispersive X-ray spectroscopy (EDS). And from the results (See Fig. S2 in the Supplementary data), we can infer that the major component of the silvery material was titanium oxide, which indicates the occurrence of tribo-oxidation at the sliding interface.

Raman spectra at three or four different positions, as indicated in Fig. 2b, were measured for each tribofilm. For the tribofilms of pure GNC film (see Fig. 2c), the shapes of Raman spectra are similar to that of the initial GNC film. All of them show sharp D and G bands, indicating the graphene nanocrystalline structure of the tribofilm. Therefore, the formation of tribofilm accompanied with graphitization, which is derived from the restructuring of graphene nanocrystallites in wear debris [6]. For the Ti-doped GNC films, the Raman spectra of the tribofilms after 300 cycles also possess sharp D-G bands. But it can be found that the

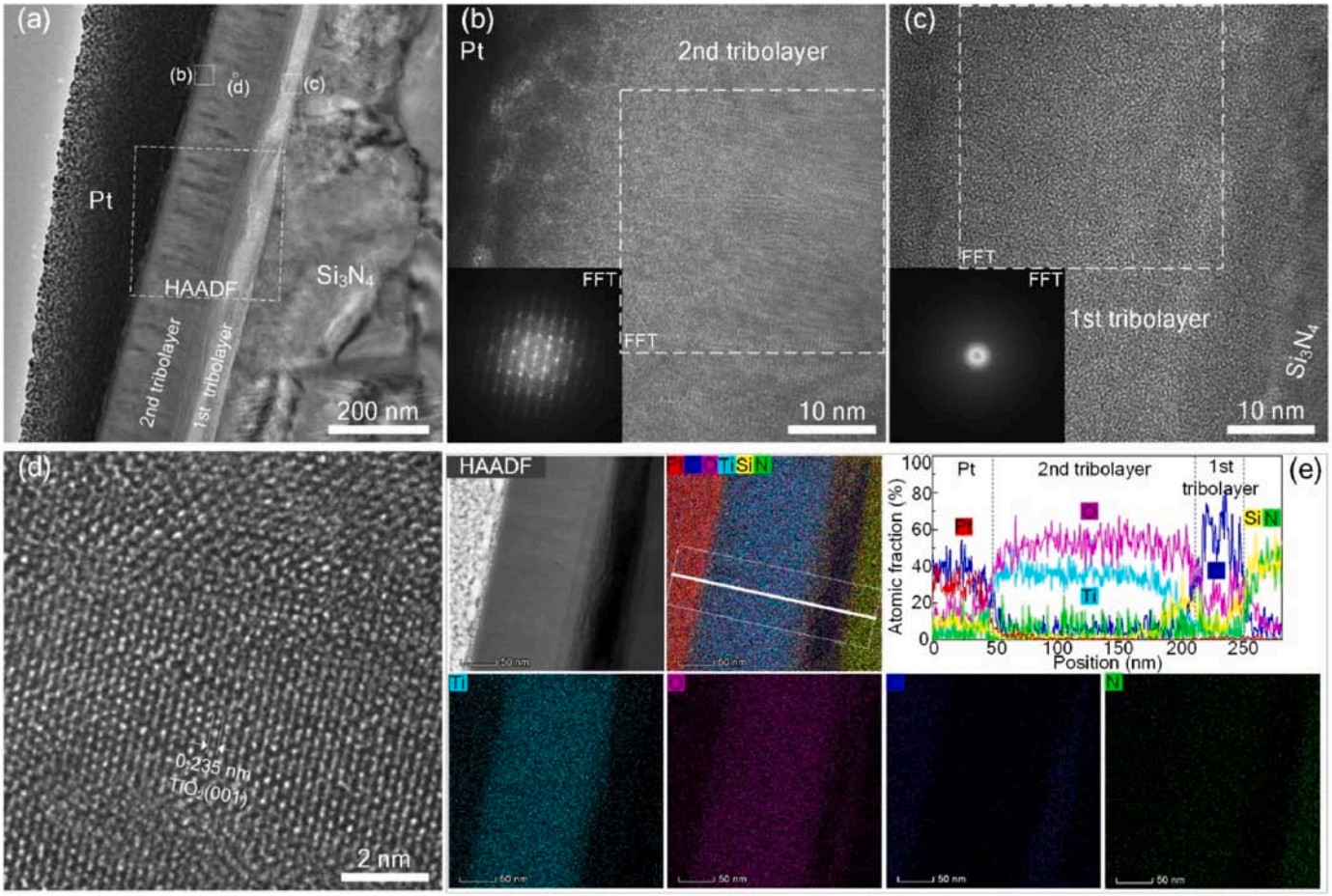

Fig. 3. (a–d) Cross-sectional TEM images and FFT images of the tribofilm after 2000 cycles of the Ti-doped GNC film (Ti target current: 0.7 A). (e) Cross-sectional view EDS results of the tribofilm. The HAADF STEM image, element concentration profiles across the tribofilm measured by EDS-line scan, Ti, O, C, N element distributions and their composite are presented. (A colour version of this figure can be viewed online.)

relative intensities of D and G bands decreased with the increase of the sliding cycles, and became indistinguishable after 2000 cycles. This suggests that the carbon content inside the tribofilm was too small to be detected, which also means the tribofilm was mainly made up of titanium oxide (silvery material). To sum up the results in Fig. 2, we can deduce that the friction behaviors of the Ti-doped GNC films were directly depended on the structure evolution of tribofilms. After run-in, friction coefficient decreased to a low friction stage due to the formation of graphitized tribofilm. Meanwhile, titanium oxide was generated through tirbo-oxidation of TiC in the air, and gradually accumulated at the sliding contact area. The titanium oxide had a competition relationship with carbon, and eventually covered the entire contact area of Si_3N_4 ball surface as sliding to a certain cycle. Thus, the tribofilm transformed from carbon to titanium oxide. And the transformation process triggered the friction-transition stage and steady-friction stage of Ti-doped GNC films. Additionally, as we know, one necessary element for the formation of titanium oxide is Ti, which is acquired from the Ti-doped GNC films. When the Ti content in the film increased, the titanium oxide accumulated faster at the ball surface. Thus, shorter periods of low-friction stage and friction-transition stage were obtained (see Fig. 2a). In short, graphitization and tribo-oxidation were in a competitive relationship at the friction interfaces of Ti-doped GNC films, resulting in the four-stage friction behavior.

The cross-sectional nanostructure of the tribofilm of the Ti-doped GNC film after 2000 cycles was observed and analyzed with TEM. The results are shown in Fig. 3. In the low-magnification TEM image (Fig. 3a), a significant double-layer tribofilm can be observed on the surface of Si_3N_4 ball. Fig. 3b–d are the enlarged TEM images of the different regions indicated in Fig. 3a. The nanostructures of the 1st tribolayer and 2nd tribolayer are amorphous and crystalline, respectively. And for the crystallites in the 2nd tribolayer, the lattice spacing in one direction is measured to be 0.235 nm, close to the d value of the TiO_2 (001) plane. Fig. 3e shows the EDS analysis results of the tribofilm. Combined with the HAADF image, element concentration profiles, and element distribution images, we can find that the 1st tribolayer is dominated by carbon and oxygen, with average contents of ~57% and ~23%, respectively. The 2nd tribolayer was dominated by oxygen and titanium, with average contents of ~53% and ~36%, respectively. Therefore, the steady friction of Ti-doped GNC film was really due to interfacial sliding between the crystalline titanium oxide surface (2nd tribolayer) and the worn Ti-doped GNC surface. And the low-friction stage is corresponded to the 1st carbon-based tribolayer. It should be noted that the nanostructure of carbon-based tribolayer is graphitized at the low-friction stage (see Fig. 2), and then transformed to amorphous carbon oxide at the steady-friction stage. These reveal the leading role of tribo-oxidation at the steady-friction stage, and further verify the competitive relationship between graphitization and tribo-oxidation. And the competition in here is more like a rat-race. Only one winner can stick to the end, as the tribo-oxidization almost replaced the graphitization at last.

3.3. Friction behaviors of AL-doped and Si-doped GNC films

Fig. 4a shows the typical friction curves of Al-doped and Si-doped

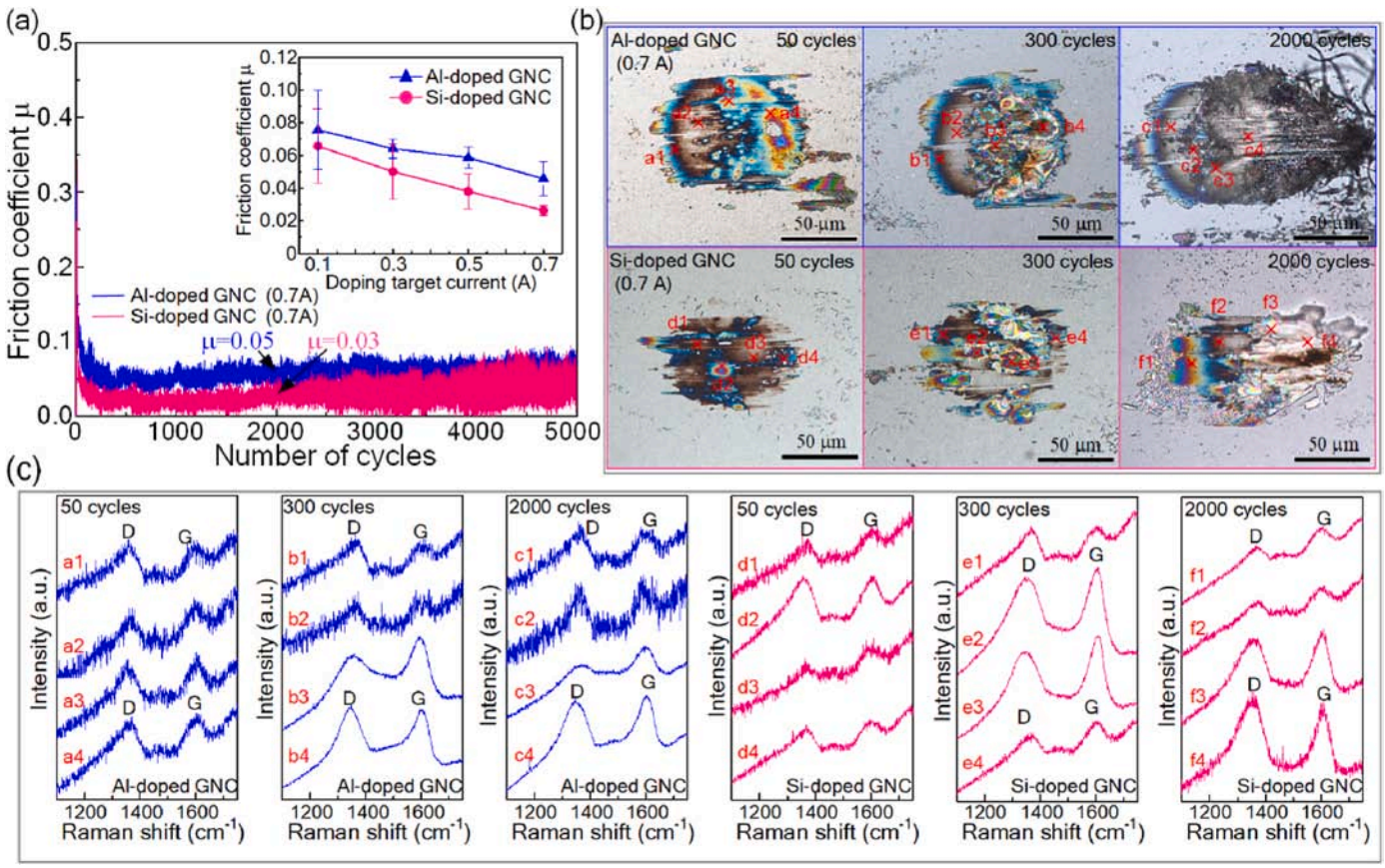

Fig. 4. (a) Typical friction curves of Al-doped and Si-doped GNC films with doping target current of 0.7 A. Inset is the friction coefficients of Al-doped and Si-doped GNC films with different doping target currents. (b) Optical images of worn scars on the Si_3N_4 ball surfaces after different sliding cycles of the Al-doped and Si-doped GNC films. (c) Raman spectra of the worn scars on the Si_3N_4 ball surfaces indicated in Fig. 4(b). (A colour version of this figure can be viewed online.)

GNC films with doping target current of 0.7 A. After run-in periods, the friction coefficients decreased to steady low values of 0.05 and 0.03, respectively. And from the inset, it can be seen that the friction coefficients decreased with the increase of doping target current. This suggest that Al and Si doping has a positive effect on the reduction of friction coefficient. The tribofilms of the Al-doped and Si-doped GNC films after different sliding cycles were observed with optical microscope, as shown in Fig. 4b. For both of the films, distinct tribofilms formed on the surfaces of the Si_3N_4 balls after 50 cycles, resulting in the decreasing of friction coefficients at the run-in stages. And for all of the tribofilms in Fig. 4b, the appearances are showing random distributions of silvery and black areas. And the results of EDS-elemental mapping analyses also exhibit non-uniform elemental distribution (See Fig. S3 and Fig. S4 in the Supplementary data). Therefore, the material distributions of the tribofilms are not uniform in the plan view. The low friction behaviors of Al-doped and Si-doped GNC films could not be solely attributed to any one substance within the tribofilms. Fig. 4c shows the Raman spectra of the tribofilms indicated in Fig. 4b. It can be found that all of the Raman spectra have D and G bands, stating the existence of graphene nanocrystallites in different areas of tribofilms. But the intensities of the D and G bands vary greatly, and they are just little higher than the background noise in some spectra. Hence, the contents of graphene nanocrystallite in different areas of the tribofilms also have great difference. The origination of low friction cannot be fully explained from the perspective of graphitization alone.

The cross-sectional nanostructure of the tribofilm of the Al-doped GNC film after 2000 cycles was observed and analyzed with TEM. The results are shown in Fig. 5. In the low-magnification TEM image (Fig. 5a), the tribofilm shows an overlapping multilayer structure. Fig. 5b–e are the enlarged TEM images of the different regions indicated in Fig. 5a. Fig. 5b–c and Fig. 5d–e shows the two main substances of the overlapping multilayer, respectively. It can be seen that the nanostructures in Fig. 5b–c are polycrystalline. Combined with the results of EDS element analysis (Fig. 5f), it can be concluded that the polycrystalline substance is inferred to be aluminium oxide from the dominated distribution of oxygen (52.3 at.%) and aluminum (35.3 at.%) in those regions. In the regions of Fig. 5d and e, carbon (56.8 at.%) and oxygen (28.9 at.%) are the major components (see Fig. 5f). The nanostructures shown in Fig. 5d and e are amorphous carbon and graphene nanocrystalline, respectively. The size of graphene nanocrystallite is very small, corresponding with the weak intensities of D and G bands in Fig. 4c. Therefore, in the cross-sectional view, the tribofilm is composed of alternating stacks of aluminium oxide layer and carbon-based layer. Further, tribo-oxidation and graphitization are coexisting in the tribofilm of Al-doped GNC film both in the plan view and in the cross-sectional view.

Fig. 6 shows cross-sectional TEM images and EDS results of the tribofilm after 2000 cycles of the Si-doped GNC film (Si target current: 0.7 A). The tribofilm has a uniform amorphous nanostructure in the cross-sectional view (see Fig. 6a–c). And from the EDS results (Fig. 6d), it can be seen that the main components of the tribofilm are O (42.3%), C (36.4%), and Si (18.5%). Thus, the dominant phenomenon is tribo-oxidation in this region. It is noticed that the TEM sample was observed in a region of only a few microns. From the analysis results of Raman spectra, the existence of graphene nanocrystallites can be confirmed in some certain regions of the tribofilm (see Fig. 4c). Therefore, for this Si-doped GNC film, tribo-oxidation and graphitization are coexisting in the tribofilm, but the tribo-oxidation play a dominant role. This dominant role is believed to be related to Si doping concentration, which is ~11.6 at.% in the Si-doped GNC film (See Fig. S1 in the

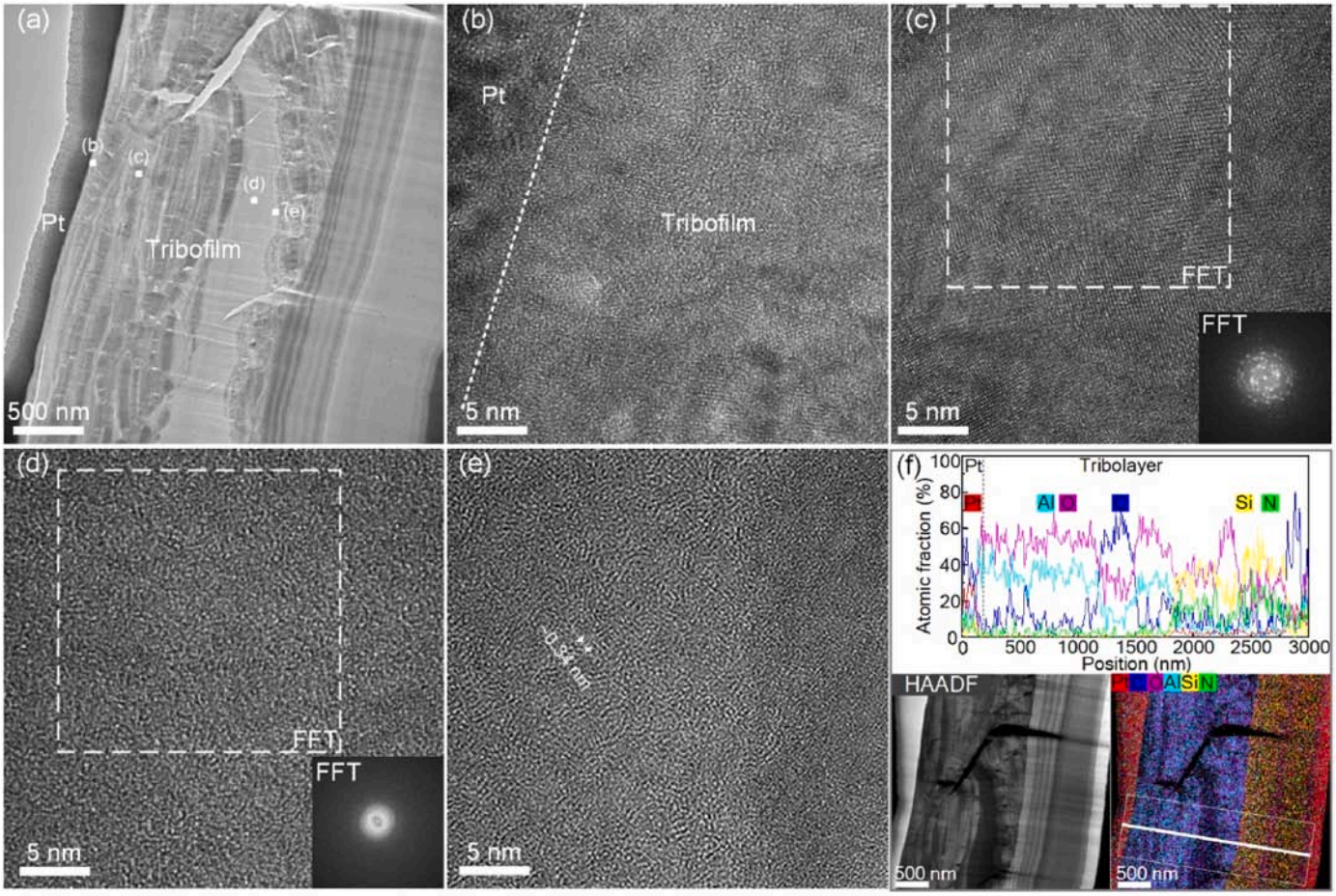

Fig. 5. (a–e) Cross-sectional TEM images and FFT images of the tribofilm after 2000 cycles of the Al-doped GNC film (Al target current: 0.7 A). (f) Cross-sectional view EDS results of the tribofilm. The HAADF STEM image, element distribution image, element concentration profiles across the tribofilm measured by EDS-line scan are presented. (A colour version of this figure can be viewed online.)

Supplementary data).

3.4. Graphitization vs tribo-oxidation

Based on the above results of friction tests and nanostructure characterizations, it is evidenced that the relationship between graphitization and tribo-oxidation is competitive in the tribofilms of Ti-doped GNC film, resulting in a staged friction behavior. For the Al-doped and Si-doped GNC films, the tribo-oxidation and graphitization are coexisting in the tribofilms, and jointly give rise to the low friction behaviors. The schematic diagram of the competitive and coexisting relationships is presented in Fig. 7. Intuitively, the relationship is depended on the type of doping element. The fundamental reason is believed to be the difference in the magnitude of friction force between the worn surface of film and the oxide induced by friction. For Ti-doped GNC film (see Fig. 2), the friction coefficient of titanium oxide (steady friction stage) is higher than that of graphene nanocrystallite (low friction stage). When the titanium oxide and graphene nanocrystallite mixed distributed in the tribofilm, the uneven local friction force in the different regions of the tribofilm resulted in a large fluctuation of friction coefficient (friction-transition stage). The high friction force region (titanium oxide) caused high heat and stress, and under these conditions the tirbo-oxidation is more intense. Oxidation of titanium would further increase the amount of titanium oxide in the tribofilm, causing the expansion of the titanium oxide region. Oxidation of carbon produced carbon monoxide or carbon dioxide, which could emit from the sliding interface under a certain oxidization degree, leading to the decline in carbon content. In consequence, the surface of tribofilm would eventually be completely covered by titanium oxide. Note that the tribofilm was quickly formed after a short run-in period, so the friction coefficient was really depended on the interfacial sliding between the tribofilm and the worn surface of film [13]. Therefore, the nanostructure transformation of the tribofilm from graphene nanocrystallite to titanium oxide in turn led to the variation of friction coefficient from ~0.05 to ~0.13 (see Fig. 2). The graphene nanocrystallite could help to lower the interaction force between the sliding surfaces from strong covalent bonds to mainly weak van der Waal forces [6,31,32]. While the titanium oxide would cause abrasive and oxidative wear [18,25], resulting in the high friction coefficient.

For the Al-doped GNC or Si-doped GNC films (see Fig. 4), the friction coefficients decreased with the increase of doping concentration, which suggests that the local friction forces of aluminum oxide and silicon-carbon oxide are close to or a little lower than that of graphene nanocrystallite. The formation of aluminum oxide or silicon-carbon oxide does not lead to a rapid oxidation consumption of carbon, so they can be in a state of equilibrium. The tribo-oxidation and graphitization are coexisting in the tribofilms, and the friction behaviors exhibited steady low friction states, as presented in Fig. 7. Certainly, the actual coexisting mechanism of tribo-oxidation and graphitization could be more complicated, which need a further discussion. When aluminum oxide slides against the carbon surface, two kinds of atomic interactions (C–O, C–Al) may form at the friction interface, which depends on the aluminum oxide is O-terminated or Al-terminated. The interaction between C and Al atoms is weak, resulting in low adhesion [33]. The

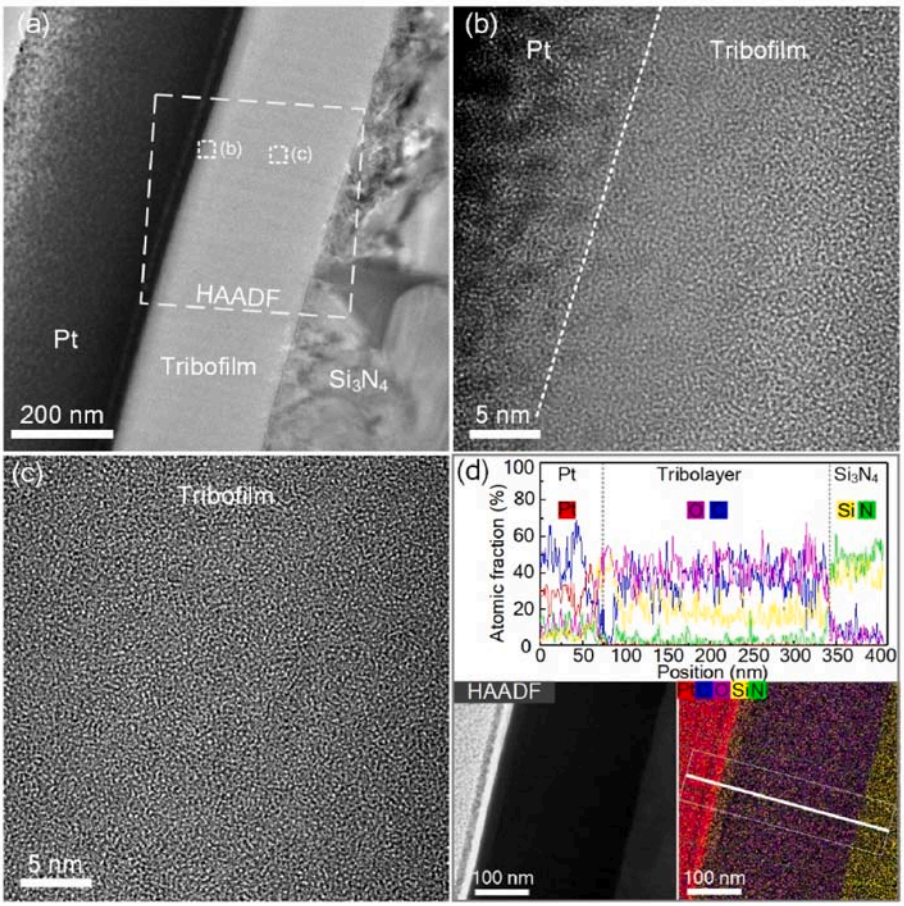

Fig. 6. (a–c) Cross-sectional TEM images of the tribofilm after 2000 cycles of the Si-doped GNC film (Si target current: 0.7 A). (f) Cross-sectional view EDS results of the tribofilm. The HAADF STEM image, element distribution image, element concentration profiles across the tribofilm measured by EDS-line scan are presented. (A colour version of this figure can be viewed online.)

interaction between C and O atoms is strong, resulting in strong adhesion [15,33]. These weak and strong atomic interactions may give rise to the alternating stacks of aluminum oxide layer and carbon-based layer during the formation of tribofilm (see Fig. 5), ensuring the sliding surface to be a weak interaction state. In addition, the graphene nanocrystalline carbon surface also has benefit to suppress the formation of the interfacial C–O and C–Al bonds due to the low reactivity of graphene sheets [15]. As a result, the local friction force of aluminum oxide could close to that of graphene nanocrystallite. When silicon-carbon oxide exists at sliding interfaces, it can interact with the humid environment through tribo-chemical effects, promoting the absorption of water with formation of hydrophilic Si–OH structure [34]. The low shear strength of this hydrophilic Si–OH structure is commonly suggested to be the major cause of low friction for Si-doped amorphous carbon films [35,36]. Hence, the local friction force of silicon-carbon oxide is close to or a little lower than that of graphene nanocrystallite. Therefore, the tribo-oxidation and graphitization can coexist in the tribofilms and jointly induce the steady low friction behaviors for the Al-doped GNC and Si-doped GNC films.

We have showed that element doping is an effective way to optimize the nanostructure and friction properties of GNC film. However, the guiding principle of this strategy should take into account the relationship between graphitization and tribo-oxidation govern by the types of doping elements. Particularly, it should be emphasized that the competitive or coexisting relationship revealed in this study is for the low concentration doping. If the doping concentration continues to rise, the graphitization of tribofilm will diminish further, and the tribo-oxidation induced by doping element or abrasive wear induced by related carbide or oxide nanocrystallites will dominate and degrade the friction performance [24,37]. In addition, note that the doped GNC films are embedded with abundant graphene nanocrystallites, which is helpful for the friction induced graphitization [6], thus the relationship between graphitization and tribo-oxidation can be clarified effectively. And owing to their unique nanostructures and friction behaviors, the doped GNC films can also be expected to have many other excellent properties, such as current-carrying friction [22], fatigue [38], and friction in a water environment [39], which will be explored in the near future.

4. Conclusions

In summary, we have studied the friction behaviors of graphene nanocrystalline carbon (GNC) films doped with different elements (Ti, Al, Si), with aim to clarify the respective effects of graphitization and tribo-oxidation on the friction behavior and the formation of tribofilm. The results revealed that the relationships between graphitization and tribo-oxidation could be competitive or coexisting, which are depended on the doping elements. For competitive type, the friction coefficient of Ti-doped GNC film first decreased to a low-friction stage due to graphitization, and then gradually increased into a steady-friction stage by tribo-oxidation. For coexisting type, the graphitization and tribo-oxidation co-induced the steady-low-friction behaviors of Al-doped and Si-doped GNC films. Our work provides new insights into the friction mechanism, which is helpful for the design and fabrication of nanostructured carbon film with desired friction behaviors.

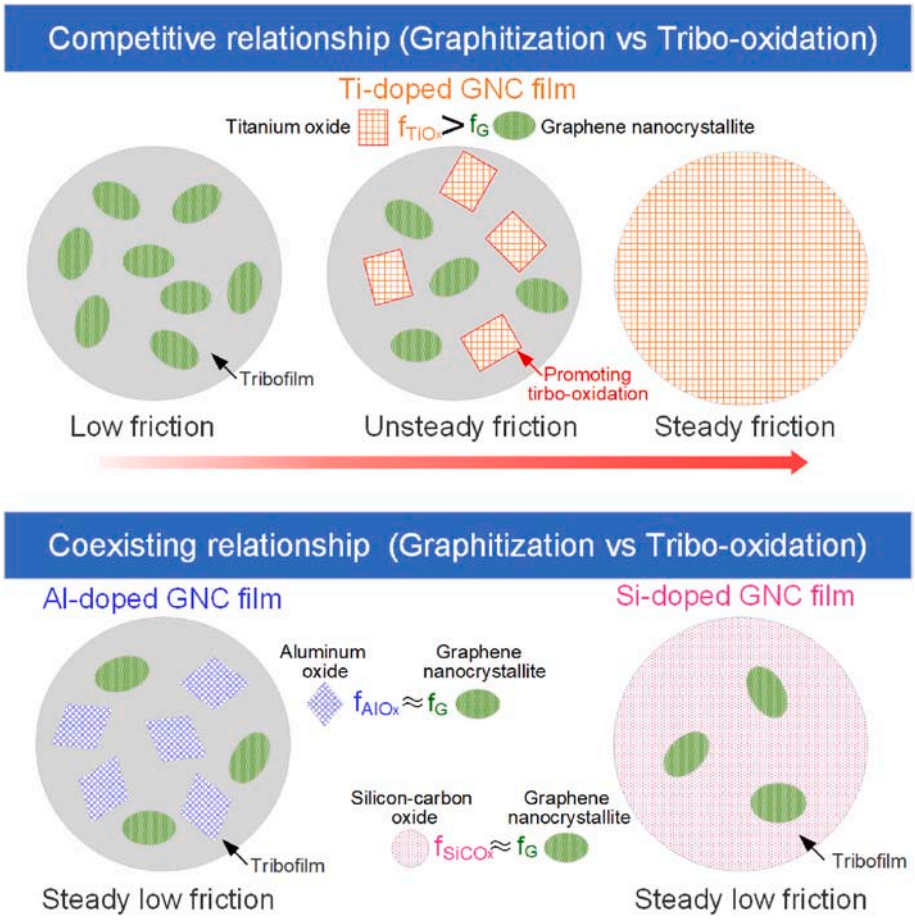

Fig. 7. Schematic diagram of the competitive and coexisting relationships between graphitization and tribo-oxidation in the tribofilms of Ti-doped GNC, Al-doped GNC and Si-doped GNC films. The local friction force of titanium oxide (f_{TiOx}) is higher than that of graphene layer (f_G). While the local friction forces of aluminum oxide (f_{AlOx}) and silicon-carbon oxide (f_{SiCOx}) are approximately equal to f_G. (A colour version of this figure can be viewed online.)

CRediT authorship contribution statement

Cheng Chen: Conceptualization, Methodology, Investigation, Visualization, Writing – original draft, Writing – review & editing, Funding acquisition. **Peidong Xue:** Investigation, Visualization, Writing – review & editing. **Dongfeng Diao:** Conceptualization, Writing – review & editing, Supervision, Funding acquisition.

Declaration of competing interest

The authors declare that they have no known competing financial interests or personal relationships that could have appeared to influence the work reported in this paper.

Acknowledgements

The authors would like to acknowledge the National Natural Science Foundation of China (Nos. 52175179 and 51975383), Natural Science Foundation of Guangdong Province (No. 2022A1515010555), and Shenzhen Fundamental Research Program (No. JCYJ20210324100406018). The Electron Microscopy Center (EMC) of Shenzhen University is kindly acknowledged for the technical supports in TEM and FIB.

Appendix A. Supplementary data

Supplementary data to this article can be found online at https://doi.org/10.1016/j.carbon.2022.07.001.

References

[1] K. Bewilogua, D. Hofmann, History of diamond-like carbon films-From first experiments to world wide applications, Surf. Coating. Technol. 242 (2014) 214–225.
[2] S.V. Hainsworth, N.J. Uhure, Diamond like carbon coatings for tribology: production techniques, characterisation methods and applications, Int. Mater. Rev. 52 (3) (2007) 153–174.
[3] K. Koji, Past, present and future of tribology in Japan, Jurnal Tribologi 20 (2019) 1–25.
[4] X. Li, B. Bhushan, Micromechanical and tribological characterization of hard amorphous carbon coatings as thin as 5 nm for magnetic recording heads, Wear 220 (1998) 51–58.
[5] Y. Wang, K. Gao, B. Zhang, Q. Wang, J. Zhang, Structure effects of sp2-rich carbon films under super-low friction contact, Carbon 137 (2018) 49–56.
[6] C. Chen, P.D. Xue, X. Fan, C. Wang, D.F. Diao, Friction-induced rapid restructuring of graphene nanocrystallite cap layer at sliding surfaces: short run-in period, Carbon 130 (2018) 215–221.
[7] X. Chen, J. Li, Superlubricity of carbon nanostructures, Carbon 158 (2020) 1–23.
[8] N. Dwivedi, R.J. Yeo, C. Dhand, J. Risan, R. Nay, S. Tripathy, et al., Boosting contact sliding and wear protection via atomic intermixing and tailoring of nanoscale interfaces, Sci. Adv. 5 (2019), eaau7886.
[9] S.H. Ramaswamy, J. Shimizu, W. Chen, R. Kondo, J. Choi, Investigation of diamond-like carbon films as a promising dielectric material for triboelectric nanogenerator, Nano Energy 60 (2019) 875–885.
[10] W.Q. Zhang, D.F. Diao, K. Sun, X. Fan, P.F. Wang, Study on friction-electrification coupling in sliding-mode triboelectric nanogenerator, Nano Energy 48 (2018) 456–463.
[11] A.P. Merkle, A. Erdemir, O.L. Eryilmaz, J.A. Johnson, L.D. Marks, In situ TEM studies of tribo-induced bonding modifications in near-frictionless carbon films, Carbon 48 (2010) 587–591.
[12] D.S. Wang, S.Y. Chang, Y.C. Huang, J.B. Wu, H.J. Lai, M.S. Leu, Nanoscopic observations of stress-induced formation of graphitic nanocrystallites at amorphous carbon surfaces, Carbon 74 (2014) 302–311.

[13] T.W. Scharf, I.L. Singer, Role of the transfer film on the friction and wear of metal carbide reinforced amorphous carbon coatings during run-in, Tribol. Lett. 36 (2009) 43–53.
[14] D.W. Kim, K.W. Kim, Effects of sliding velocity and normal load on friction and wear characteristics of multi-layered diamond-like carbon (DLC) coating prepared by reactive sputtering, Wear 297 (2013) 722–730.
[15] Y. Wang, J. Xu, J. Zhang, Q. Chen, Y. Ootani, Y. Higuchi, et al., Tribochemical reactions and graphitization of diamond-like carbon against alumina give volcano-type temperature dependence of friction coefficients: a tight-binding quantum chemical molecular dynamics simulation, Carbon 133 (2018) 350–357.
[16] X. Li, A. Wang, K.R. Lee, Fundamental understanding on low-friction mechanisms at amorphous carbon interface from reactive molecular dynamics simulation, Carbon 170 (2020) 621–629.
[17] X. Chen, C. Zhang, T. Kato, X. Yang, S. Wu, R. Wang, et al., Evolution of tribo-induced interfacial nanostructures governing superlubricity in a-C:H and a-C:H:Si films, Nat. Commun. 8 (2017) 1675.
[18] K.P. Shaha, Y.T. Pei, D. Martinez-Martinez, JThM. De Hosson, Influence of surface roughness on the transfer film formation and frictional behavior of TiC/a-C nanocomposite coatings, Tribol. Lett. 41 (2011) 97–101.
[19] O. Wilhelmsson, M. Rasander, M. Carlsson, E. Lewin, B. Sanyal, U. Wiklund, et al., Design of nanocomposite low-friction coatings, Adv. Funct. Mater. 17 (2007) 1611–1616.
[20] S.G. Zhou, L.P. Wang, Z.B. Lu, Q. Ding, S.C. Wang, R.J.K. Wood, et al., Tailoring microstructure and phase segregation for low friction carbon-based nanocomposite coatings, J. Mater. Chem. 22 (2012) 15782–15792.
[21] K. Sun, X. Fan, W. Zhang, P.D. Xue, D.F. Diao, Contact-focusing electron flow induced nanosized graphene sheets formation in amorphous carbon film for fast low-friction, Carbon 149 (2019) 45–54.
[22] K. Sun, D. Diao, Current density effect on current-carrying friction of amorphous carbon film, Carbon 157 (2020) 113–119.
[23] A.A. Gharam, M.J. Lukitsch, Y. Qi, A.T. Alpas, Role of oxygen and humidity on the tribo-chemical behaviour of nonhydrogenated diamond-like carbon coatings, Wear 271 (2011) 2157–2163.
[24] D. Nilsson, N. Stavlid, M. Lindquist, S. Hogmark, U. Wiklund, The role of aluminum additions in the oxidation and wear of a TaC:C low-friction coating, Surf. Coating. Technol. 203 (2009) 2989–2994.
[25] D.D. Kumar, N. Kumar, S. Kalaiselvam, R. Radhika, A.M. Rabel, R. Jayavel, Tribo-mechanical properties of reactive magnetron sputtered transition metal carbide coatings, Tribol. Int. 114 (2017) 234–244.
[26] C. Kong, P. Guo, L. Sun, Y. Zhou, Y. Liang, X. Li, et al., Tribological mechanism of diamond-like carbon films induced by Ti/Al cooping, Surf. Coating. Technol. 342 (2018) 167–177.
[27] C. Chen, X. Fan, D.F. Diao, Ultrasmooth nanocrystalline carbon film induced by low concentration doping: carbide disorienting graphene nanocrystallite, Carbon 158 (2020) 69–76.
[28] C. Wang, D.F. Diao, X. Fan, C. Chen, Graphene sheets embedded carbon film prepared by electron irradiation in electron cyclotron resonance plasma, Appl. Phys. Lett. 100 (2012), 231909.
[29] D. Graf, F. Molitor, K. Ensslin, C. Stampfer, A. Jungen, C. Hierold, et al., Spatially resolved Raman spectroscopy of single- and few-layer graphene, Nano Lett. 7 (2007) 238–242.
[30] L.M. Malard, M.A. Pimenta, G. Dresselhaus, M.S. Dresselhaus, Raman spectroscopy in graphene, Phys. Rep. 473 (5–6) (2009) 51–87.
[31] T.B. Ma, Y.Z. Hu, H. Wang, Molecular dynamics simulation of shear induced graphitization of amorphous carbon films, Carbon 47 (2009) 1953–1957.
[32] S.W. Liu, H.P. Wang, Q. Xu, T.B. Ma, G. Yu, C. Zhang, et al., Robust microscale superlubricity under high contact pressure enabled by graphene-coated microsphere, Nat. Commun. 8 (2017), 14029.
[33] R.H. Zhang, Z.B. Lu, L. P Wang, Understanding the run-in tribological behavior of amorphous carbon films against Al2O3 balls under high vacuum, RSC Adv. 5 (2015) 32690–32697.
[34] S. Kajita, M.C. Righi, Insigths into the tribochemistry of silicon-doped carbon-based films by Ab initio analysis of water–surface interactions, Tribol. Lett. 61 (2016) 17.
[35] J. Choi, S. Nakao, M. Ikeyama, T. Kato, Effect of oxygen plasma treatment on the tribological properties of Si-DLC coatings, Phys. Status Solidi 5 (2008) 956–959.
[36] X. Chen, T. Kato, M. Nosaka, Origin of superlubricity in a-C:H:Si films: a relation to film bonding structure and environmental molecular characteristic, ACS Appl. Mater. Interfaces 6 (2014) 13389–13405.
[37] D. Martínez-Martínez, C. López-Cartes, A. Fernández, J.C. Sánchez-López, Influence of the microstructure on the mechanical and tribological behavior of TiC/a-C nanocomposite coatings, Thin Solid Films 517 (2009) 1662–1671.
[38] X. Li, B. Bhushan, Development of a nanoscale fatigue measurement technique and its application to ultrathin amorphous carbon coatings, Scripta Mater. 47 (2002) 473–479.
[39] D.C. Sutton, G. Limbert, D. Stewart, R.J.K. Wood, The friction of diamond-like carbon coatings in a water environment,, Friction 1 (2013) 210–221.